Available online at www.sciencedirect.com
ScienceDirect
Journal of Power Sources 161 (2006) 692–701
JOURNAL OF POWER SOURCES
www.elsevier.com/locate/jpowsour

The influence of hydrogen intercalation on inner pressure of Ni/MH battery during fast charge

Jianzhen Shi, Feng Wu *, Daozhong Hu, Shi Chen, Licai Mao, Guoqing Wang

School of Chemical Engineering and Environment, Beijing Institute of Technology, Beijing 100081, China

Received 5 December 2005; received in revised form 30 March 2006; accepted 4 April 2006
Available online 12 June 2006

Abstract

Gaseous hydrogen is confirmed to be the main component and primarily responsible for the inner pressure rise inside the 8-Ah Ni/MH batteries during fast charge. Based on a temperature-dependent pressure model proposed in this work, the kinetic characteristics of the hydrogen evolution were investigated. The overpotential and exchange current density were obtained by fitting the presented equation to the experimental data. Moreover, the profiles of hydrogen concentration during fast charge was further modeled and calculated according to the proposed mathematical model of hydrogen intercalation. It is indicated that diffusion step controls the fast charge performances and the higher the charge rate is, the more quickly the negative electrode attains to the maximum surface intercalation fraction, and however, the calculated results also show that further charge can reduce the difference of charge efficiency among the various rate during fast charge. Numerical investigations also reveal that the increase of diffusion coefficient and decrease of the particle size can efficiently improve the characteristics of fast charge, respectively.

Keywords: Ni/MH battery; Hydrogen intercalation; Inner pressure

1. Introduction

Nickel-metal hydride batteries are now the preferred power source for hybrid electric vehicle (HEV) because of the high specific power, specific energy and perfect integrated features. The high power Ni/MH batteries emphasized by HEVs inevitably encounter fast charge in the actual operation. Owing to the electrochemistry of Ni/MH batteries, however, fast charge is a complicated and serious challenge under the actual status. Fast charge will lead to a remarkable rise in temperature and an increased pressure buildup inside the Ni/MH batteries.

The pressure buildup is a result of gas accumulation from the side reaction during charge, and the amount of charge consumed by the side reaction can be related to the inner pressure, which is determined by both the kinetics of the processes occurring at the MH electrode/electrolyte interface and the rate of hydrogen intercalation within the bulk of the MH alloy. While the temperature variation in the battery during fast charge and its influence on the pressure profile and hydrogen intercalation is thus naturally concerned [1]. Additional gaseous hydrogen could be released from the bulk of the hydride because of higher equilibrium hydrogen pressure of the hydride electrode under higher temperature. A remarkable increase in temperature can also lead to an acceleration of hydrogen-evolution reaction; hence, more gaseous hydrogen could escape from the electrode, even leak through release valve under higher pressure, resulting in undue capacity loss at the negative electrode, which in turn, will cause capacity imbalance between the two electrodes. As a result, a noticeable temperature rise could lead to an accelerated pressure buildup inside the batteries. Therefore, in high temperature accompanied by high pressure, charging efficiency as well as battery properties may deteriorate.

Efforts have been made to investigate the hydrogen diffusion and inner pressure in Ni/MH batteries [1–6], but the effects of temperature and the gradient of chemical potential (GCP) on the hydrogen intercalation and inner pressure were not considered in modeling the hydrogen diffusion process and inner pressure profiles. In this paper, the gaseous hydrogen was firstly confirmed to be dominant gas component by the experiment, and a temperature-dependent pressure model and a temperature/GCP-dependent hydrogen intercalating model were proposed to inves-

* Corresponding author. Tel.: +86 10 68912528; fax: +86 10 68451429.
E-mail addresses: stonesjz@vip.163.com, wufeng863@vip.sina.com (F. Wu).

0378-7753/$ – see front matter © 2006 Elsevier B.V. All rights reserved.
doi:10.1016/j.jpowsour.2006.04.076

Nomenclature

a	particle radius (mm)
a_H	activity of hydrogen in the hydride alloy
A	heat-dissipating area (m^2)
b	defined in Eq. (15)
c	concentration of gaseous hydrogen ($mol\,m^{-3}$)
C	hydrogen concentration in the alloy ($mol\,m^{-3}$)
C_0	initial hydrogen concentration in the alloy ($mol\,m^{-3}$)
C_{max}	maximal hydrogen concentration in the alloy ($mol\,m^{-3}$)
C_p	specific heat capacity ($J\,kg^{-1}\,K^{-1}$)
D	diffusion coefficient ($m^2\,s^{-1}$)
D_{ref}	reference diffusion coefficient ($m^2\,s^{-1}$)
E_H	activation energy of hydrogen evolution reaction ($kJ\,mol^{-1}$)
E_{MH}	activation energy of MH electrode charge ($kJ\,mol^{-1}$)
F	Faraday constant ($C\,mol^{-1}$)
f_H	hydrogen fugacity
h	convection heat-transfer coefficient ($W\,m^{-2}\,K^{-1}$)
i	applied current density of charge ($A\,m^{-2}$)
I	applied discharge current (A)
j	current density for hydrogen evolution ($A\,m^{-2}$)
j_0	exchange current density for hydrogen evolution ($A\,m^{-2}$)
$j_{0,ref}$	exchange current density for hydrogen evolution at reference temperature ($A\,m^{-2}$)
J	applied charge current (A)
P	inner pressure (Pa)
P_{eq}	equilibrium pressure (atm)
q	heat generation rate per unit volume ($W\,m^{-3}$)
Q_0	capacity of the charged negative electrode (Ah)
r	radial coordinate (m)
R	universal gas constant ($8.314\,J\,mol^{-1}\,K^{-1}$)
R_{int}	internal resistance (mΩ)
t	time (s)
T	temperature (°C)
T_∞	ambient temperature (°C)
T_0	initial temperature (°C)
T_{ref}	reference temperature (°C)
U	battery voltage (V)
U_0	open-circuit voltage (V)
V	battery volume (m^3)
x	dimensionless radial coordinate
y	intercalation fraction of hydrogen
y_{ave}	average fraction of hydrogen intercalation

Greek symbols

α	charge transfer coefficient
ε	free space fraction inside a battery (%)
η	overpotential (V)
Λ	specific area of MH electrode ($m^2\,m^{-3}$)
ρ	average density ($kg\,m^{-3}$)
τ	transition time corresponding to zero intercalation fraction of hydrogen (s)

tigate the kinetics of hydrogen evolution and the variation of hydrogen intercalation during fast charge, respectively. Finally, a sensitivity analysis was also performed to assess the effects of diffusion coefficient and the alloy particle size on the characteristics of rapid charge, respectively.

2. Experimental

All experiments were performed on the cylindrical 8-Ah Ni/MH batteries fabricated in our laboratory and the apparatus was shown in Fig. 1. The battery with a gas hole was sealed in a stainless steel container, and the detailed information of the batteries can be found in Ref. [7]. Arbin BT cycler was used to control the process of charging under the constant current condition. The data of current, voltage and inner pressure were recorded. In order to determine accurately the inner pressure and the gas composition, two cycles were thus carried out, one for recording the inner pressure, another for analysing the evolved gas during charge.

Gas analysis was conducted on a GC112 gas chromatograph (Analytical Instrument Ltd., Shanghai, China). The Ultra high purity argon was used as carrier gas at a flow rate of 30 ml min^{-1}. The column oven was isothermally held to be 30 °C. The injector and detector were kept at 40 and 50 °C, respectively. The volume of 0.5 ml of gas was fetched each time to test gas content.

3. Results and discussion

3.1. Analysis of gas components

The result from gas chromatography was shown as Fig. 2. During 1*C* rate (8*A*) charge, gaseous hydrogen content rises with charging time and subsequently rises up to the peak value at the end of charge. The gaseous hydrogen content decreases

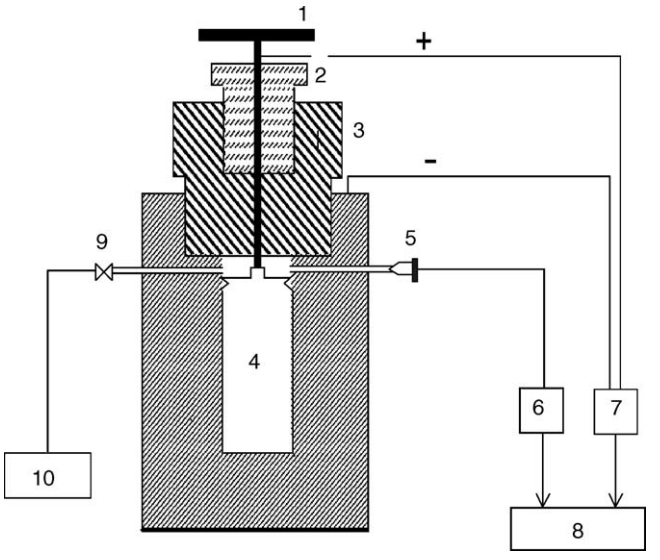

Fig. 1. Schematic diagram of the apparatus for inner pressure and gas analysis. 1: Positive post; 2: screw cap; 3: sealed cap; 4: battery; 5: pressure sensor; 6: indicator; 7: battery cycler; 8: computer; 9: injecting valve; 10: gas chromatograph.

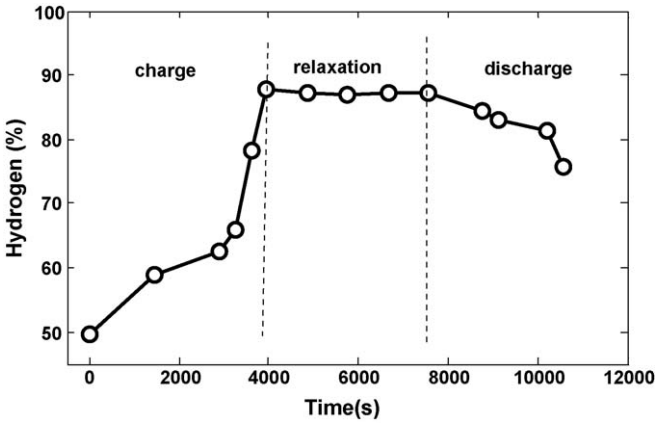

Fig. 2. Hydrogen content variation during 1*C* rate cycle.

slowly during the relaxation periods, followed by a slightly rapid drop during discharge. It is obvious that hydrogen gas becomes the dominant component and oxygen gas is only possessed of a small portion of the total gas when the battery was charged at 1*C* rate even when discharged. It is indicated that hydrogen gas predominates in the evolved gas from Ni/MH battery under high rate of charge. It has been frequently reported (for example [8,9]) that the hydrogen pressure inside the Ni/MH batteries was found to increase significantly during overcharge because the diffusion of adsorbed atomic hydrogen to the bulk of hydrogen storage alloy is not sufficiently faster than the adsorbed atomic hydrogen formation reaction Eq. (1), at the end of charge and during overcharge, the accumulated hydrogen on the surface of MH electrode trends to a peak value, the hydrogen can thus not quickly diffuse into the bulk MH alloy, gaseous hydrogen thus increasingly evolves shown as Eq. (2) [10], and in turn the inner pressure dramatically increases shown in Fig. 3. Although the capacity of negative electrode in this study is 40% higher than that of positive electrode, during overcharge, gaseous hydrogen still increasingly evolves because of a low diffusion coefficient of hydrogen, in nature. Inevitably, hydrogen evolution would further rise in high-rate charging [1]:

$$M + H_2O + e^- \rightarrow OH^- + MH \quad (1)$$

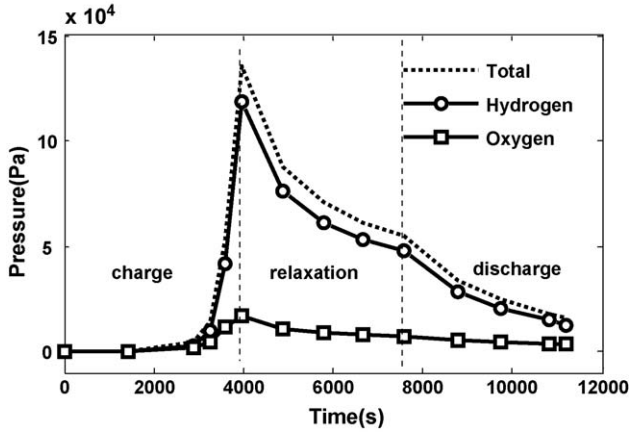

Fig. 3. Inner pressure profiles inside the batteries during 1*C* charge and discharge.

$$MH + H_2O + e^- \rightarrow OH^- + H_2 + M \quad (2)$$

It can also be seen that oxygen gas is possessed of considerable proportion in the gas phase during incipient charge period, this means that oxygen gas ceaselessly releases from nickel electrode even at the beginning of charge. This result is in agreement with the research of Bourgault and Conway [11]. However, the rate of oxygen evolution is likely suppressed and so small that the primary charging reaction predominates at the positive electrode during normal charge periods [1].

On the other hand, at the end of charge and during overcharge period, oxygen gas should evolve in a higher rate at the positive electrode, i.e. a higher oxygen gas content or a higher partial pressure of oxygen, but it can be seen that oxygen gas is only still possessed of small ratio during the overcharge, hence, it is deduced that oxygen recombination is probably fast at the negative electrode, and in turn reduces the gaseous oxygen which transfers from the positive electrode to the negative electrode through the separator and electrolyte. Wu et al. [12] and Yang and Liaw [13] proposed oxygen recombination equation as Eq. (3). In contrast to the desired result, however, during the relaxation periods, the content of gaseous hydrogen drops at a small rate, which indicates that hydrogen recombination on the positive electrode, is very torpid compared to the oxygen recombinant at the negative electrode. Hydrogen recombination reaction was shown as Eq. (4) [13]. Micro-calorimetric [14,15], XRD/TEM [16] and electrochemical techniques [17], together with huge amount of experiences accumulated in works associated with Ni–H_2 batteries [18], clearly indicate that the rate of recombination of hydrogen at the positive electrode is a relatively slow process [4]:

$$2H_2O + O_2 + 4e^- \rightarrow 4OH^- \quad (3)$$

$$1/2H_2 + OH^- \rightarrow H_2O + e^- \quad (4)$$

The inner pressure profiles of the battery were presented as Fig. 3. The inner pressure is very small at the begging of charge period, and rises tardily up to 0.1 atm before 90% input charge, however, an quick jump in the pressure appears after about 90% charge input, followed by a dramatical rise until reaching the peak pressure of 1.4 atm at the end of charge in a short time.

The 2*C* rate charge was also conducted in our laboratory, and the similar results have been achieved. According to the gas chromatography, it is concluded that the hydrogen content increases with charge rates, and therefore the higher charging rate the battery was charged, the higher partial pressure of hydrogen the system got, while gaseous oxygen content decreases with an increase in charge rates. It is thus reasonable that at high charge rate, the oxygen pressure can be omitted, and only hydrogen pressure was considered in the following calculation.

3.2. Temperature variation with charge time

3.2.1. Estimation of total inner resistance

Fig. 4 plots the voltage profiles of an 8-Ah Ni/MH battery at 1*C*, 2*C* and 4*C* rates, respectively. The voltage–current curves are then transformed into the plotting for the battery voltage

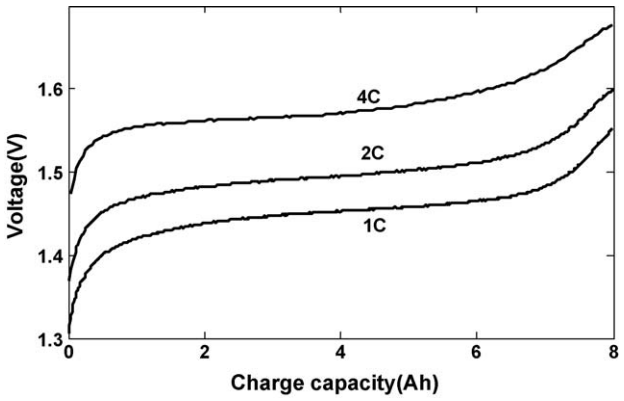

Fig. 4. Voltage curves during 1*C*, 2*C* and 4*C* rates charge.

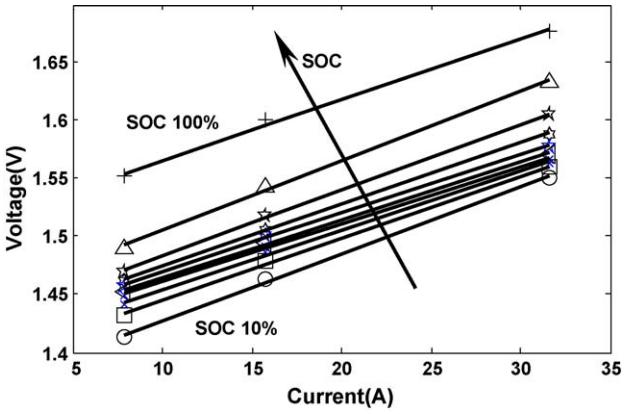

Fig. 5. Relationship between charging voltage and charging currents.

with respect to the charge rate (current) under the different state of charge (SOC) as Fig. 5, which illustrates that the voltage exhibits a perfect linear correlation with the charge rate. The total inner resistance, equaling to the slope of the voltage versus current (Fig. 6), is then obtained according to Fig. 5. The inner resistance variation is summarized in Fig. 6. It can be seen that the resistance slightly fluctuates with charge process. Owing to the small range of the resistance variation during all the charge periods, i.e. the inner resistance is weakly dependent on charge

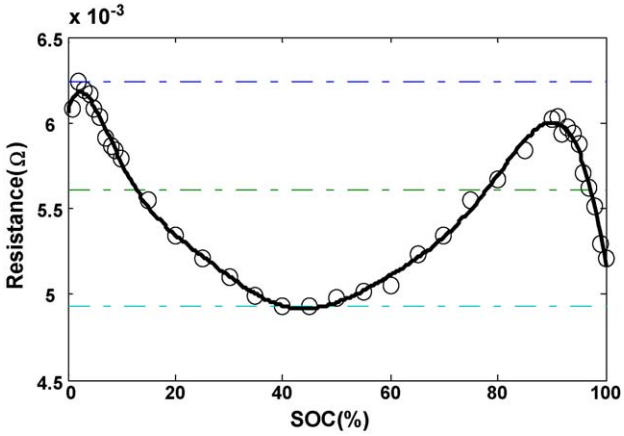

Fig. 6. Variation of inner resistance with SOC during charge.

process, therefore for simplicity, an average inner resistance is adopted to be 5.6 mΩ according to Fig. 6. It was believed that the influence of this simplification on the calculated accuracy was expected to be enough small, and hence the fluctuation can be negligible. The above mentioned inner resistance is used to calculate the irreversible heat during fast charge periods.

3.2.2. Temperature variation during fast charge periods

In our earlier work [7], the temperature profiles across the battery during fast charge have been investigated and obtained the detailed results. In this work, an average effect of the temperature on the inner pressure is concerned for simplicity. It was expected that the final accuracy was not obviously affected by this treatment. Thus the following transient differential equation describes the variation of temperature in the battery system,

$$\rho C_p \frac{\mathrm{d}T}{\mathrm{d}t} = \frac{Ah}{V}(T_\infty - T) + q = \frac{m}{V}(T_\infty - T) + q \tag{5}$$

where T refers to the temperature, q is the volumetric heat generation rate, ρ represents the volume averaged density, C_p denotes the specific heat, V and A are the battery volume and surface area, respectively, T_∞ is the ambient temperature, and h is the thermal transfer coefficient. For simplicity, according to the assumption of Bernard et al. [19], the heat generation rate is assumed to be distributed uniformly throughout the battery using the volume-averaging approach under the assumption that no phase change is involved and only electrochemical/intercalation reactions exist in the Ni/MH battery, hence heat generation rate can be written as

$$q = \frac{J}{V}\left(JR_{\mathrm{int}} + T\frac{\mathrm{d}U_0}{\mathrm{d}T}\right) \tag{6}$$

where, R_{int} denotes the battery inner resistance, U_0 is the open-circuit voltage of a battery, J is the applied current. The heat generation rate generally consists of the joule heat J^2R_{int} (irreversible) and the reversible heat effect ($JT\mathrm{d}U_0/\mathrm{d}T$). According to Ref. [20], the temperature coefficient ($\mathrm{d}U_0/\mathrm{d}T$) of the battery is presented as

$$\frac{\mathrm{d}U_0}{\mathrm{d}T} = \frac{\mathrm{d}U_{\mathrm{p},0}}{\mathrm{d}T} - \frac{\mathrm{d}U_{\mathrm{n},0}}{\mathrm{d}T} \tag{7}$$

where the first term on the right side denotes the positive electrode temperature coefficient, the second term represents the negative electrode temperature coefficient. The initial condition during normal charge can be written as follows:

$$T = T_0 \,\mathrm{at}\, t = 0 \tag{8}$$

When a battery was overcharged, q consists of the joule heat and the oxygen recombination heat at the hydride electrode, according to Ref. [21].

$$q = \frac{J}{V}(1.48 + JR_{\mathrm{int}}) \tag{9}$$

The first term refers to the oxygen recombinant heat at the hydride electrode, and the second term arises from ohmic heat from the battery inner resistance R_{int}, which is equal to the value of inner resistance at 100% input charge based on the data from

Table 1
Parameters for thermal calculation

Parameters	Values
Battery density (kg m^{-3}), ρ	3900 [7]
Initial temperature (°C), T_0,	25
Reference temperature (°C), T_{ref}	25
Heat capacity (J kg^{-1} K^{-1}), C_p	1882 [7]
Battery volume (m^3), V	4.83×10^{-5}
Heat-dissipating area (m^2), A	7.64×10^{-3}
Positive electrode temperature coefficient (V K^{-1}), $dU_{p,0}/dT$	-1.35×10^{-3} [12]
Negative electrode temperature coefficient (V K^{-1}), $dU_{n,0}/dT$	-1.55×10^{-3} [12]

Fig. 5. According to the above transient differential equation and the initial conditions, the following solutions can be obtained. These solutions mean the temperature variation with charge time during charge and overcharge periods, respectively. The required parameters for temperature calculation are listed in Table 1.

The solution of temperature for normal charge is written as follows:

$$T = \frac{mT_0 + J^2R_{int}}{m - bJ} - \frac{JbT_0 + J^2R_{int}}{m - bJ}\exp\left(-\frac{m - bJ}{V\rho C_p}t\right)$$
$$\approx T_0 + \frac{J(JR + bT_0)}{V\rho C_p}t - \frac{J(JR + bT_0)(m - bJ)}{2(V\rho C_p)^2}t^2$$
$$\left(\frac{m - bJ}{V\rho C_p}t \ll 1\right) \quad (10)$$

The solution of temperature for overcharge can be written as follows:

$$T = T_{end} + \frac{1.48J + J^2R_{int}}{m}\left\{1 - \exp\left[-\frac{m}{V\rho C_p}(t - t_{end})\right]\right\}$$
$$\approx T_{end} + \frac{1.48J + J^2R_{int}}{V\rho C_p}(t - t_{end})$$
$$-\frac{m(1.48J + J^2R_{int})}{2(V\rho C_p)^2}(t - t_{end})^2 \quad \left(\frac{m}{V\rho C_p}t \ll 1\right) \quad (11)$$

Based on Eqs. (10) and (11), Fig. 7 can be obtained, which illuminates the temperature variations at the different rates during fast charge. It can be seen that the temperature rises are obvious, especially at higher rates and under overcharge. For example, the average temperature of the system rises about 30 °C at the end of 4C rate charge. These results are consistent with the average temperature of the accurate thermal modeling [7], which indicates that this simplified treatment is very reliable. A remarkable rise in temperature can firstly expand the inner pressure inside the batteries in the same condition, more important, strongly affect the rate of electrochemical reaction and increase the gas content in the batteries, i.e., exchange current density of gaseous hydrogen evolution increases with the battery temperature. The mentioned two aspects can significantly influence the rate of gas evolution, especially the latter, hence, in turn strongly affecting the inner pressure profiles inside the battery, the temperature variation should be thus considered in investigating the inner pressure of the battery in fast charge regime.

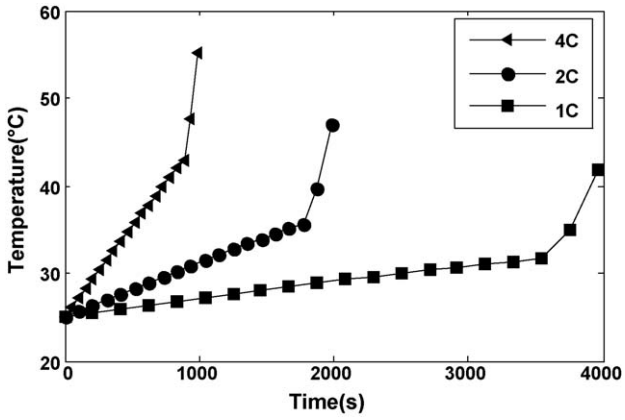

Fig. 7. Temperature variation during different charge periods.

3.3. Description of the inner pressure

Inoue et al. [10] assumed that hydrogen evolution at the negative electrode is most attributed to Eq. (2) and it could act like a reversible electrode.

According to the results of the gas chromatography, the contribution of oxygen pressure can reasonably negligible when compared with hydrogen contribution to the battery inner pressure, hence, the inner pressure of the battery is mainly characterized by hydrogen evolution reaction. It is assumed that the gaseous hydrogen is uniformly profiled across the unoccupied space inside the battery [22,23], and thus the gaseous hydrogen concentration and pressure are independent of space inside the battery, then the hydrogen concentration is obtained by solving Fick's second law:

$$\varepsilon\frac{dc}{dt} = \frac{j\Lambda}{F} \quad (12)$$

where c is the gaseous hydrogen concentration, ε denotes the ratio of gas space to the battery volume, t the time, j the current density of hydrogen evolution reaction, Λ the specific area of MH electrode particles, and F is the Faraday constant. The pressure P can be denoted as

$$P = cRT = \frac{RT\Lambda}{\varepsilon F}\int j\,dt \quad (13)$$

The Butler–Volmer kinetic expression is assumed to describe the charge transfer processes occurring across the MH electrode/electrolyte interface. Accordingly, the current density of gaseous hydrogen evolution reaction can be thus written by

$$j = 2j_0\sinh\left(\frac{\alpha F\eta}{RT}\right) \quad (14)$$

where j_0 denotes the exchange current density and η is the surface overpotential devoted to driving hydrogen evolution reaction. The charge transfer coefficient, α is taken to be equal to 0.5. The overpotential η is not available in literature and in experimental. Liaw and Yang [1] found that the overpotential of hydrogen

evolution is linear with charging time, i.e., $\eta = bT$, then the inner pressure can be written as follows:

$$P = cRT = \frac{2j_0R^2T^2\Lambda}{\varepsilon b\alpha F^2}\left[\cosh\left(\frac{\alpha F\eta}{RT}\right) - 1\right] \quad (15)$$

The above equation is only obtained without considering the factor of temperature, but at higher rates, the effect of temperature could not be neglected. The Arrhenius type expression is adopted to describe the temperature dependence of the exchange current density:

$$j_0 = j_{0,\mathrm{ref}} \exp\left[-\frac{E_\mathrm{H}}{R}\left(\frac{1}{T} - \frac{1}{T_\mathrm{ref}}\right)\right] \quad (16)$$

where $j_{0,\mathrm{ref}}$ presents the exchange current density at the reference temperature of T_ref, E_H denotes the activation energy of the hydrogen evolution reaction. The above equation implies that j_0 increases with the system temperature. A linear temperature and time dependent overpotential was further modified to describe the overpotential variation during fast charge:

$$\eta = bt + (T - T_0)\frac{\mathrm{d}U_{\mathrm{n},0}}{\mathrm{d}T} \quad (17)$$

The battery pressure can be thus rewritten as Eq. (18), which was utilized to fit the experimental pressure with the charging time when substituting Eqs. (16) and (17) into Eq. (15):

$$P = \frac{2j_{0,\mathrm{ref}}R^2T^2\Lambda}{\varepsilon\alpha bF^2}\exp\left[\frac{E_\mathrm{H}}{R}\left(\frac{1}{T_0} - \frac{1}{T}\right)\right]\left[\cosh\left(\frac{F\alpha\eta}{RT}\right) - 1\right] \quad (18)$$

The activation energy of the reaction for hydrogen evolution is assumed to be 50 kJ mol^{-1}. This assumption is based on a fact that the amount of gaseous hydrogen accumulated in the battery is trivial compared to the total charge input even when overcharged, because of a smaller unoccupied space and a limited pressure inside the actual battery, therefore the reaction for hydrogen evolution is deduced to be more difficult than the reaction for MH electrode charge according to the actual electrochemical efficiency during fast charge. The activation energy of the charge reaction of the MH electrode is 30 kJ mol^{-1} [13]. The temperature coefficient is assumed to be equal to that of the MH electrode.

It can be observed that the effects of temperature on the pressure inside the battery are mainly characterized by exponential rises of exchange current density and electrochemical polarization. The required parameters for fitting the inner pressure are listed in Table 2.

The pressure profiles at different rates are compared in Fig. 8, which indicates the larger the rate, the earlier the pressure buildup is witnessed. Fig. 8 also shows the fitting of the pressure modeled by Eq. (18) to the experimental data during 1C, 2C, 4C rates charge, the values of b's in Eq. (18) are averagely equal to 1.41×10^{-4}, 2.45×10^{-4} and 3.09×10^{-4} V s^{-1} at 1C, 2C, 4C rates charge, respectively, and the values of reference exchange current density averagely change from 1.39×10^{-10} at 1C rate and 1.82×10^{-10} at 2C rate to 3.87×10^{-9} A cm^{-2} at 4C rate. The disparity in exchange current density under different rate was probably yielded by unavoidable instrumental error under lower charge rates, at which hydrogen evolution rate is so small that the fitted results were underestimated. Therefore, the exchange current density at 4C rate is expected to be close to the real value. On the other hand, it can also be observed that the fitting at higher rate is better than that at lower rate, indicating the result at high rate is more reliable than that at low rate.

Table 2
Parameters for inner pressure and hydrogen intercalation

Parameters	Values
Specific area of MH electrode (m^2 m^{-3}), Λ	4.5×10^5
Particle radius (m), a	5×10^{-6}
Molecular weight of MH alloy (g mol^{-1}), W	419
Density (kg m^{-3}), ρ	7.49×10^3
Free space fraction (%), ε	0.10
Initial intercalation fraction of hydrogen (%), y_0	0.10
Activation energy of H_2 evolution (kJ mol^{-1}), E_H	50
Activation energy of MH electrode (kJ mol^{-1}), E_MH	30 [13]

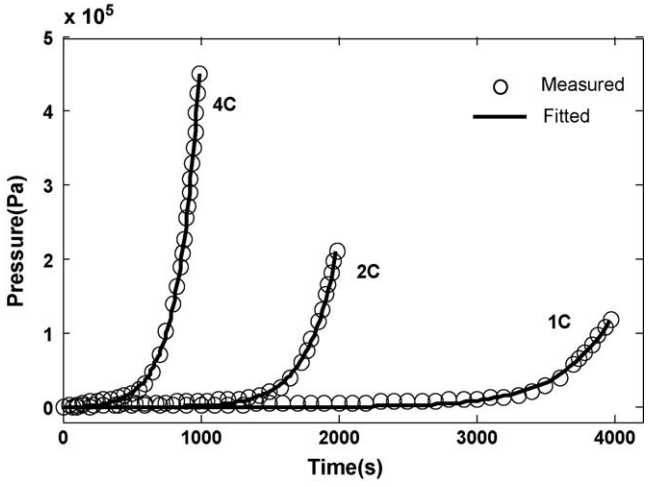

Fig. 8. Fitting the model to the experimental pressure at various charging rates.

Fig. 9 shows the changes of exchange current density and overpotential during 4C rate fast charge. The exchange current density of hydrogen evolution reaction rises distinctly up to

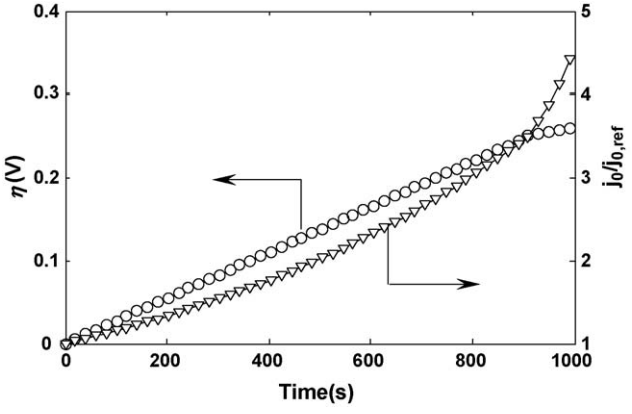

Fig. 9. The variation of exchange current density and overpotential during 4C rate charge.

4.5 times that of the reference state owing to a constant rise in system temperature. It is observed that the reaction polarization constantly increases until overcharge periods where the overpotential rises evenly due to a steeper rise in temperature. Thus, the effects of temperature on the inner pressure profile is significant under fast charge conditions, indicating temperature variation in the system can not be neglected even if only qualitative agreement with the experimental data is sought during high rates charge. The remarkable disparity of kinetic characteristics would consequentially be resulted when neglecting the temperature factor under high rates charge.

3.4. The profiles of hydrogen intercalation

Compared with the total charge input, the charge for hydrogen accumulation inside the battery is smaller due to the smaller unoccupied space and limited reaction kinetics of hydrogen evolution in the actual battery. This means the effect of gaseous hydrogen reaction on the MH alloy charge can be negligible. Therefore, the hydrogen intercalation can be treated by the Fick's secondary law. It is assumed that the MH electrode particles are in spherical form with a mean radius of a, the hydrogen intercalating fraction (relative concentration) in the MH negative electrode satisfies the diffusion equation:

$$\frac{\partial y(x,t)}{\partial t} = \frac{1}{x^2}\frac{\partial}{\partial x}\left(\frac{x^2}{a^2}D\frac{\partial y(x,t)}{\partial x}\right) \tag{19}$$

$$y = \frac{C}{C_{\max}}, \qquad x = \frac{r}{a} \tag{20}$$

where, the dependent variables are time t and the radial coordinate r, which is the spherical direction from the center of a particle. D is the diffusion coefficient, C is the hydrogen concentration, $C_{\max}$ corresponds to the maximum hydrogen concentration in the alloy, y and x are dimensionless concentration and radial distance from the center to the surface of a particle, respectively. The boundary and initial conditions can be written as Eqs. (21) and (22), respectively:

$$D\frac{\partial y(x,t)}{\partial x}\bigg|_{x=1} = \frac{ai}{FC_{\max}}; \qquad D\frac{\partial y(x,t)}{\partial x}\bigg|_{x=0} = 0 \tag{21}$$

$$y(x,0) = \frac{C_0}{C_{\max}} = y_0 \tag{22}$$

where i is the applied current density of charge, C_0 is the initial concentration of hydrogen; the above boundaries imply that there is no flux of hydrogen in the core of the particle, while the constant flux of hydrogen was deposited onto the surface of the alloy particle in the constant current charging regime. And y_0 means a particle of initially uniform intercalation profile.

When the hydrogen intercalation approaches the maximum content, the boundary can be modified as

$$y(x,t)|_{x=1} = 1; \qquad D\frac{\partial y(x,t)}{\partial x}\bigg|_{x=0} = 0 \tag{23}$$

The above boundary means that on the surface of MH electrode the constant intercalated fraction, equaling to the maximum intercalated fraction, was adopted after the top content, while there exists no flux of hydrogen in the core of the particle. The new initial condition corresponds to the state at the top intercalation.

The diffusion coefficient is taken to be dependent on the temperature of system and the intercalating fraction in MH alloy:

$$D = \frac{D_{\text{ref}}}{f(y)}\exp\left[\frac{E_{\text{MH}}}{R}\left(\frac{1}{T_{\text{ref}}} - \frac{1}{T}\right)\right] \tag{24}$$

where E_{MH} is the activity energy of charging MH electrode, D_{ref} is the reference diffusion coefficient at the reference temperature T_{ref}. The factor $f(y)$, reflecting effect of the gradient of the chemical potential on hydrogen intercalation [5,24,25], is defined as

$$f(y) = \frac{\mathrm{d}\ln a_{\text{H}}}{\mathrm{d}\ln y} = \frac{\mathrm{d}\ln f_{\text{H}}}{2\,ln\,y} \approx \frac{1}{2}\frac{\mathrm{d}\ln P_{\text{eq}}}{\mathrm{d}\ln y} \tag{25}$$

where a_{H} is the activity of hydrogen in the hydride alloy, f_{H} and P_{eq} are the hydrogen fugacity and the hydrogen equilibrium pressure corresponding to the equilibrium state. Fig. 10 shows the P–C–T curves of the typically commercial AB_5-type alloy consisting of $MmNi_{3.55}Co_{0.75}Mn_{0.4}Al_{0.3}$ [19], which is the same as that of the alloy employed in the studied batteries. The hydrogen content under 1 atm is more important for practical applications as negative electrodes of Ni/MH battery since the effective hydrogen capacity of the alloy is utilized only under about 1 atm of hydrogen pressure [26]. Thus, the effective hydrogen uptake of the alloy reaches approximately to AB_5H_5, corresponding to an electrochemical capacity of 320 mAh g^{-1}, which is very close to the actual top specific capacity of the alloy used in the experimental battery. The above P–C–T curve is then fitted to obtain the mathematical formula of $f(y)$ as a function of the intercalation fraction of hydrogen.

In the MH electrode, the average hydrogen intercalation fraction y_{ave}, is defined to be the same as the average intercalation in a particle according to the property of assumed spherical particle. Then, at any given charging time, there exists the following integral:

$$y_{\text{ave}} = 3\int_0^1 x^2 y\,\mathrm{d}x \tag{26}$$

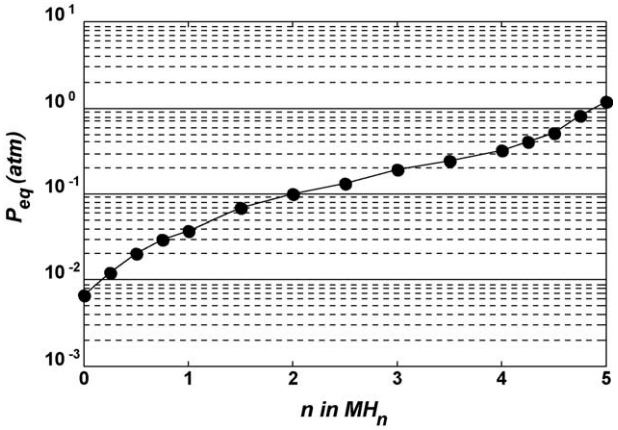

Fig. 10. P–C–T curve of AB_5 alloy [19].

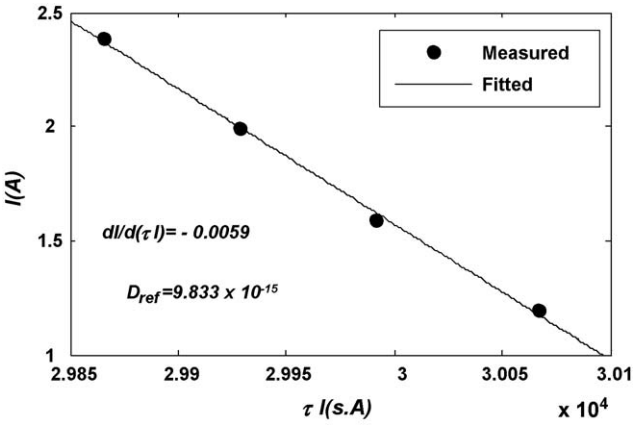

Fig. 11. Relationship between I and $I\tau$ under small current discharge.

The reference diffusion coefficient D_{ref} can be calculated by Eq. (27) [6,27] when the applied current density is smaller and the thermal effect could thus be avoided,

$$\frac{D_{\text{ref}}}{a^2}(Q_0 - I\tau) = \frac{I}{15} \tag{27}$$

where I is the discharged current, τ the transition time corresponding to the time when the hydrogen intercalation fraction approaches zero, and Q_0 the capacity of the charged electrode. Eq. (27) is valid for small constant discharge currents which leads to a larger amount of hydrogen released from the alloy particle. Fig. 11 shows a well linear relationship between I and $I\tau$ at various discharge currents, the diffusion coefficient of hydrogen is thus estimated to be 9.83×10^{-15} m^2 s^{-1} with a particle radius of 5 μm. Table 2 lists the values of the parameters required in the modeling of hydrogen intercalation in the MH electrode.

FEMLAB® software system is adopted to solve the above partial differential equations based on the above initial and boundary conditions. The intercalation fraction variations of hydrogen during various charging currents are indicated in Fig. 12. The intercalation fraction of hydrogen on the surface is maximal at the time of 3700, 1655 and 700 s during 1C, 2C and 4C rate charge, respectively. This calculation is in agreement with the experimental measurements (Fig. 8) in spite of a slight

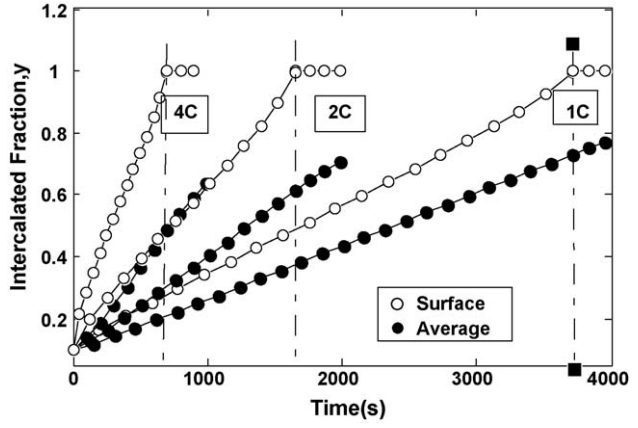

Fig. 12. Calculated hydrogen intercalation fraction at various charging rates.

long predicted time at 1C rate charge. It is indicated that the hydrogen increasingly evolves from the MH electrode when the surface hydrogen intercalation tends to the peak value. With hydrogen evolution, more and more charge is consumed to generate hydrogen rather than charge the active materials, thus reducing the charge efficiency, the pressure buildup inside the batteries is thus accelerated. Further imposition of the large current will be not helpful to the charge reaction. It is clearly shown that the hydrogen intercalation dominates and limits the fast charge properties, the larger current density the battery is charged, the smaller capacity density the battery obtains before the maximum surface hydrogen intercalation is reached.

The average hydrogen intercalation in the MH electrode is also shown in Fig. 12. The average intercalation of hydrogen decreases with the rise in charge rate before the top hydrogen content in the MH electrode, It is indicated that the total charging efficiency drops at higher rates, therefore the charged capacity at higher rates is less than that at lower rates before the top intercalation. However, in order to achieve full capacity in the MH electrode, further charge is practically required despite higher pressure and higher temperatures are resulted in the actual operation. During sequential charge periods, the surface intercalated fraction of hydrogen is constantly kept to be the top value. At the time close to the top intercalation, the average intercalated fractions under 1C, 2C and 4C rate charge are 72%, 62% and 46%, while the values at the end of charge rise up to 76%, 70% and 65%, respectively. The values at 1C, 2C and 4C rate charge rise 5.5%, 14.8% and 41%, respectively, which accelerates the reduction of the intercalation difference among the various rates under further charge. It is concluded that, during further charge with the same overcapacity, the charge efficiency is higher at higher rate wherein the higher pressure and temperature are probably helpful to accelerate hydrogen intercalation into the alloy matrix, especially at the higher temperature. However, overcharge should severely be controlled within the endurable duration of the batteries to avoid the high temperature and pressure, which probably lead to the battery failure. The numerical modeling suggested that, for fast charge and achieving better performances, smaller current should be imposed to charge the battery when the hydrogen intercalation tends to the top value, which can avoid the high rate of hydrogen evolution and maintain the higher charge efficiency throughout the charge process.

Based on the proposed model, the numerical calculation for the effect of diffusion coefficient on the hydrogen intercalation can be conducted. Fig. 13 depicts the effect of the measured diffusion coefficient on the surface hydrogen intercalation fraction during 4C rate charge with the particle size of 5 μm. The time to reach the maximum surface hydrogen content rises with the diffusion coefficients, which indicates more amount of hydrogen is intercalated into the alloy, and the inner pressure inside the batteries is accordingly decreased at the same charging current. It is thus naturally advantageous to increase the diffusion coefficient in improving the charging efficiency of the negative electrode as well as in alleviating the inner pressure inside the batteries.

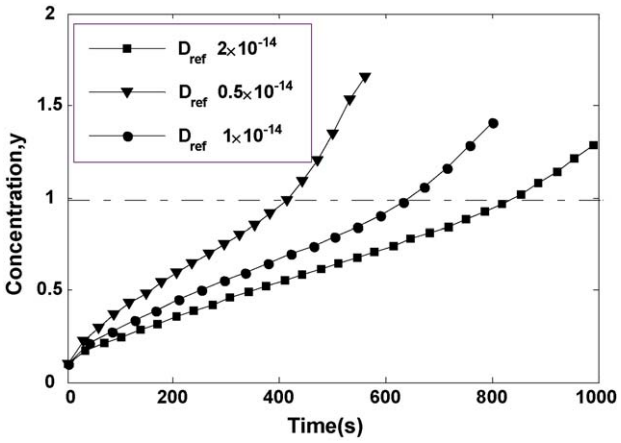

Fig. 13. Surface hydrogen intercalation at varying the measured diffusion coefficient.

It can be observed from the proposed model that the size of the particle could influence the reaction kinetics of hydrogen intercalation reaction in the alloy electrode. Therefore, the analysis of the effect of particle size on hydrogen intercalation was also performed as Fig. 14. It is indicated that the decrease of particle size can facilitate the hydrogen intercalation into the negative electrode. It is a simple consequence of the fact that, for the same porosity, an electrode with smaller particle size of alloy has larger specific surface area and the shorter time of hydrogen diffusion due to the smaller diffusion distance. Normally, when the MH negative electrode is cycled in charge and discharge, the particle sizes tends to decrease due to fracturing caused by absorption and desorbtion of hydrogen. From this point of view, it is seemed that the hydrogen diffusion kinetics may be improved when cycling the battery. However, because the conductivity of the solid matrix decreases with decreasing particle size [28], hence, the smallest particles can not give the best electrode properties, moreover, this effect becomes more pronounced when charged at higher rates. Furthermore, this kind of fracturing could also result in the incompact electrode structure, therefore, it is noticed that the results from the model cannot infinitely be true, the conductivity of the electrode and choose of particle size should be compatibly considered based on the actual state. The simulated results from the model only gives a better understanding about the effect of particle size on the hydrogen intercalation.

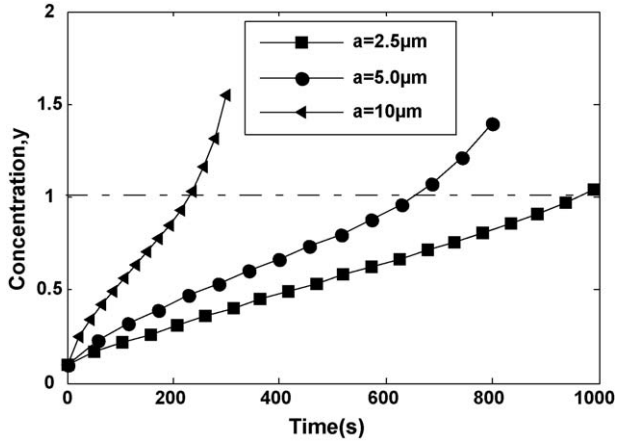

Fig. 14. Effect of particle size on the surface intercalation of hydrogen.

4. Conclusions

Gas chromatography was performed and confirmed that gaseous hydrogen is the dominant component and the inner pressure rise is primarily characterized by the hydrogen evolution reaction in the 8-Ah nickel/metal hydride batteries. The hydrogen evolution kinetics was analysed, and overpotential and exchange current density were obtained by fitting the temperature-dependent pressure model proposed in this work to the experimental measurement. Furthermore, the profiles of hydrogen intercalation during fast charge were numerically modeled according to the proposed mathematical model of hydrogen diffusion. The results indicate that the hydrogen intercalating rate in the MH electrode limits fast charge properties of the electrode, and the higher rate the battery is charged, the faster the negative electrode approaches the maximum surface concentration of hydrogen, and the higher the inner pressure is built inside the battery. The numerical modeling suggested that the characteristics of fast charge can be efficiently improved by increasing diffusion coefficient and decreasing the particle size of the alloy to some extent.

Acknowledgments

This work was supported by the National Key Basic Research and Development Program of China (grand no. 2002CB211800), and the National EV (863) key Program of China (grand no. 2003AA501231). The authors are grateful to Prof. Cun-Mao Hong of Peking University for his knowledgeable comments on this work.

References

[1] B.Y. Liaw, X.G. Yang, Electrochim. Acta 47 (2001) 875.
[2] B.Y. Liaw, X.G. Yang, Solid State Ionics 152–153 (2002) 217.
[3] X.G. Yang, B.Y. Liaw, J. Power Sources 101 (2001) 158.
[4] J. Zhang, J. Yu, C. Cha, H. Yang, J. Power Sources 136 (2004) 180.
[5] S.W. Feldberg, J.J. Reilly, J. Electrochem. Soc. 144 (1997) 4260.
[6] G. Zheng, B.N. Popov, R.E. White, J. Electrochem. Soc. 142 (1995) 2695.
[7] J. Shi, F. Wu, S. Chen, C. Zhang, J. Power Sources, in press.
[8] K. Kanda, M. Yamamoto, K. Kanno, Y. Satoh, H. Hayashida, M. Suzuki, J. Less-common Metals 174 (1991) 1227.
[9] T. Sakai, A. Yuasa, H. Ishikawa, H. Miyamura, N. Kuriyama, J. Less-common Metals 174 (1991) 1194.
[10] H. Inoue, K. Yamataka, Y. Fukumoto, C. Iwakura, J. Electrochem. Soc. 143 (1996) 2527.
[11] P.L. Bourgault, B.E. Conway, Can. J. Chem. 37 (1959) 292.
[12] B. Wu, M. Mohammed, D. Brigham, R. Elder, R.E. White, J. Power Sources 101 (2001) 149.
[13] X.G. Yang, B.Y. Liaw, J. Electrochem. Soc. 151 (2004) A265.
[14] Z. Mao, A. Visintin, J. Appl. Electrochem. 22 (1992) 409.
[15] A. Visintin, A. Anani, S. Srinivasan, A.J. Appleby, J. Appl. Electrochem. 25 (1995) 833.
[16] N. Sac Epée, B. Beaudoin, V. Pralong, T. Jamin, J.-M. Tarascon, J. Electrochem. Soc. 146 (1999) 2346.
[17] V. Pralong, N. Sac Epée, S. Taunier, B. Beaudoin, T. Jamin, A. Delahaye-Vidal, J. Electrochem. Soc. 146 (1999) 2382.

[18] NASA, Handbook for Nickel–Hydrogen Batteries, NASA Publication 1314, 1993.
[19] D. Bernardi, E. Pawlikowski, J. Newman, J. Electrochem. Soc. 132 (1985) 5.
[20] P.M. Gomadam, Electrochemical–Thermal modeling of Lithium-ion batteries, PhD Thesis, UMI, MI, 2003.
[21] N. Sato, K. Yagi, JASE Rev. 21 (2000) 205.
[22] D.M. Bernardi, M.K. Carpenter, J. Electrochem. Soc. 142 (1995) 2631.
[23] J. Newman, W. Tiedemann, J. Electrochem. Soc. 144 (1997) 3081.
[24] G.G. Botte, R.E. White, J. Electrochem. Soc. 148 (2001) A54.
[25] E. Wicke, H. Bbrodowski, in: G. Alefeld, J. Volkl (Eds.), Topics in Applied Physica, vol. 29, Springer-Verlag, NewYork, 1978, pp. 73–155 (and references therein).
[26] W.K. Hu, J. Alloys Compd. 297 (2000) 206.
[27] J. Grank, The Mathematics of Diffusion, Oxford press, London, 1976.
[28] J.M. Heikonen, H.J. Ploehn, R.E. White, J. Electrochem. Soc. 145 (1998) 1840.